SUPERDIRECTIVE 3-ELEMENT ARRAY FOR ADAPTIVE BEAMFORMING

H.J. Chaloupka[*], X. Wang[*] and J.C. Coetzee[**]

[*]Department of Electrical Engineering and Information Technology, University of Wuppertal, Rainer-Gruenter Str. 21, D-42119, Wuppertal, Germany

[**] Department of Electrical and Computer Engineering, National University of Singapore, 4 Engineering Drive 3, Singapore 117576

ABSTRACT: A small array composed of three monopole elements with very small element spacing on the order of λ/6 to λ/20 is considered for application in adaptive beamforming. The properties of this 3-port array are governed by strong mutual coupling. It is shown that for signal-to-noise maximization, it is not sufficient to adjust the weights to compensate for the effects of mutual coupling. The necessity for a RF-decoupling network (RF-DN) and its simple realization are shown. The array with closely spaced elements together with the RF-DN represents a superdirective antenna with a directivity of more than 10 dBi. It is shown that the required fractional frequency bandwidth and the available unloaded *Q* of the antenna and RF-DN structure determine the lower limit for the element spacing.

Key words: Superdirective arrays, adaptive beamforming, mutual coupling

1. INTRODUCTION

The number of mutually orthogonal radiation patterns (MORPs) associated with an antenna array equals the number of its (operational) radiation elements, *M*. Adaptive digital beamforming with *M*-1 degrees of freedom is based on a linear combination of these array-specific MORPs with variable complex-valued weights. A choice of element spacing substantially smaller than $\lambda/2$ results in strong mutual coupling, which gives rise to severe frequency bandwidth and efficiency limitations [1]-[3].

This letter addresses these problems for a specific array composed of three identical monopole antennas with an array footprint diameter of $\lambda/20$ to $\lambda/6$. The array produces three MORPs associated with three distinct eigenmodes: one low-order quasi-omni-directional pattern and two degenerated higher-order patterns. It is shown that a reduction of element spacing results in both an

increased radiation quality factor of the higher-order patterns and an increased deviation between the low- and higher-order pattern radiation resistance. Without a decoupling-network, the low-order and higher-order modes cannot be simultaneously matched, resulting in a signal-to-noise degradation, which cannot be compensated for by digital beamforming. By choice of a proper monopole height, the decoupling network reduces to simple reactive cross coupling between the antenna ports. In this way simultaneous matching of all three modes can be achieved, resulting in an optimum signal-to-noise ratio (SNR). In this new configuration, the two higher-order radiation patterns become superdirective. The allowed minimum element spacing is governed by the required fractional frequency bandwidth.

2. PROPERTIES OF 3-ELEMENT ARRAY

The array structure comprising of three monopole antenna elements is depicted in Fig. 1. The frequency-dependent admittance matrix **Y** characterises the mutual coupling between the elements of the array, and according to

$$\begin{bmatrix} I_1 \\ I_2 \\ I_3 \end{bmatrix} = \begin{bmatrix} Y_{11} & Y_{12} & Y_{12} \\ Y_{12} & Y_{11} & Y_{12} \\ Y_{12} & Y_{12} & Y_{11} \end{bmatrix} \begin{bmatrix} V_1 \\ V_2 \\ V_3 \end{bmatrix} \tag{1}$$

relates the port-currents I_n to the driving port-voltages V_n. Port voltages may be expressed as a linear combination of the orthogonal eigenvectors of the admittance matrix:

$$\begin{bmatrix} V_1 \\ V_2 \\ V_3 \end{bmatrix} = \begin{bmatrix} 1 \\ 1 \\ 1 \end{bmatrix} \frac{v_A}{\sqrt{3}} + \begin{bmatrix} 2 \\ -1 \\ -1 \end{bmatrix} \frac{v_B}{\sqrt{6}} + \begin{bmatrix} 0 \\ 1 \\ -1 \end{bmatrix} \frac{v_C}{\sqrt{2}} = \mathbf{U} \begin{bmatrix} v_A \\ v_B \\ v_C \end{bmatrix} \tag{2}$$

with v_m as the *mode-voltages*. The port currents then become

$$\begin{bmatrix} I_1 \\ I_2 \\ I_3 \end{bmatrix} = Y_A \begin{bmatrix} 1 \\ 1 \\ 1 \end{bmatrix} \frac{v_A}{\sqrt{3}} + Y_B \begin{bmatrix} 2 \\ -1 \\ -1 \end{bmatrix} \frac{v_B}{\sqrt{6}} + Y_C \begin{bmatrix} 0 \\ 1 \\ -1 \end{bmatrix} \frac{v_C}{\sqrt{2}} = \mathbf{U} \begin{bmatrix} Y_A & 0 & 0 \\ 0 & Y_B & 0 \\ 0 & 0 & Y_C \end{bmatrix} \begin{bmatrix} v_A \\ v_B \\ v_C \end{bmatrix}, \tag{3}$$

with eigenvalues $Y_A = G_A + jB_A = Y_{11} + 2Y_{12}$ and $Y_B = Y_C = G_B + jB_B = Y_{11} - Y_{12}$ as the frequency dependent *mode-admittances*. The three mutually orthogonal far-field radiation patterns associated with the eigenmodes can be characterised by the three vector functions $\mathbf{C}_m(\theta, \phi)$, normalized such that

$$\oint \mathbf{C}_l(\theta,\phi)\cdot\mathbf{C}_m^*(\theta,\phi)\,d\Omega = 4\pi\delta_{lm} \tag{4}$$

where δ_{lm} denotes the Kronecker delta function.

In order to study the effect of a change in the element spacing *a* on the frequency response of the mode-admittances $Y_A(f)$ and $Y_B(f)$ and on the corresponding radiation patterns, numerical simulations were carried out with the computer codes SuperNEC Lite [4] and Zeland IE3D [5]. In these simulations, the metallic ground plane was assumed to be infinite in size and metallic losses were neglected. In the presentation of the obtained results, f_0 and $\lambda_0 = c/f_0$ denote the *reference frequency* and the corresponding free space wavelength. The monopole length and monopole diameter were chosen as $l = \lambda_0/4$ and $d = \lambda_0/40$. The element spacing was varied between $a = \lambda_0/20$ and $a = \lambda_0/6$. For the numerical simulations, a reference frequency of $f_0 = 2.45$ GHz was chosen, but the obtained results were normalized to allow conclusions to be drawn for arbitrary operating frequencies. In Figs. 2 and 3, the results for relatively small element spacing $a = \lambda_0/10$ are shown as an example. Fig. 2 depicts the normalized radiation patterns $|\mathbf{C}_m(\pi/2,\phi)|/\sqrt{D_m}$, $m = A,B,C$ at $f = f_0 = c/4l$. The maximum directivity for the three modes were computed to be $D_A = |\mathbf{C}_A|^2_{\max} = 3.24 \equiv 5.1$ dBi, $D_B = |\mathbf{C}_B|^2_{\max} = 7.94 \equiv 9$ dBi and $D_C = |\mathbf{C}_C|^2_{\max} = 7.76 \equiv 8.9$ dBi. As a consequence of mutual coupling, mode admittance Y_A for the lower-order mode *A* with dipole-like radiation pattern substantially differs from the mode input admittance $Y_B = Y_C$ of the degenerated higher-order modes *B* and *C*. Fig. 3 shows the frequency dependence of the modal admittances as a function of the normalized frequency f/f_0. The low-order and higher-order modes resonate at different frequencies, but the most notable difference is in the radiation quality factor Q_{rad}, where the higher-order modes display a significantly higher value. The relation between the radiation quality factor of higher-order modes and the element spacing a/λ_0 is shown in Fig. 4, indicating a sharp increase with reduced spacing.

From an inspection of the numerical results, it was found that for $a < \lambda_0 / 6$, the radiation patterns can be approximated by the following analytical expressions derived under the assumption of a sinusoidal line current distribution along the monopole axes while employing a Taylor series approximation:

$$\mathbf{C}_A(\theta,\phi) \approx 1.82 \exp(j\psi_A) \frac{\cos\left(\frac{\pi}{2}\cos\theta\right)}{\sin\theta}\ \mathbf{e}_\theta \tag{5a}$$

$$\mathbf{C}_B(\theta,\phi) \approx 2.83 \exp(j\psi_B) \cos\left(\frac{\pi}{2}\cos\theta\right)\sin\phi\ \mathbf{e}_\theta \tag{5b}$$

$$\mathbf{C}_C(\theta,\phi) \approx 2.83 \exp(j\psi_C) \cos\left(\frac{\pi}{2}\cos\theta\right)\cos\phi\ \mathbf{e}_\theta \tag{5c}$$

ψ_A, ψ_B and ψ_C in eqs. (5) are phase angles that depend on the frequency.

3. EFFECTS OF MUTUAL COUPLING

By means of the eigenmode representation, the actual array with three mutually coupled elements can formally be replaced with a set of three equivalent antennas with radiation patterns corresponding to the three MORPs. In the receive mode, each of the three equivalent antennas can be modelled by means of a current source (see left part of Fig. 5) with source admittance equal to the corresponding mode admittance $Y_m = G_m + jB_m$ and source current i_m, which in case of a spectrum of homogeneous plane waves incident on the antenna becomes

$$i_m = \lambda \sqrt{\frac{G_m}{\pi Z_0}} \oint \mathbf{C}_m(\theta,\phi) \cdot \mathbf{E}_{\text{inc}}(\theta,\phi)\, d\Omega, \quad m = A, B, C \tag{6}$$

For digital beamforming, three receiver channels with input admittance Y_{in} are connected to the three antenna ports. Consequently the load in the equivalent circuits for the three modes in Fig. 5 has a value of Y_{in}, too. Due to the orthogonality of the voltage vectors defined in eq. (2), the total power delivered to the receiver channels is the sum of the power received by the three modes. In case of a power mismatch (i.e. $Y_m^* \neq Y_{\text{in}}$), the power delivered by eigenmode *m* is reduced by a factor of $|\Lambda_m|^2$ compared to the total power available from that mode, where

$$\Lambda_m = \frac{2\sqrt{G_m G_{\text{in}}}}{Y_m + Y_{\text{in}}}. \tag{7}$$

This is equivalent to a reduction in gain of the receiver channels with respect to this mode. Due to mutual coupling, the mode admittance Y_A substantially differs from $Y_B = Y_C$. If (theoretically) lossless two-port matching networks as shown in Fig. 6(a) are inserted between the antenna ports and the three receiver channels, the mode admittances Y_A, Y_B and Y_C are transformed to new admittances $\tilde{Y}_A$, $\tilde{Y}_B$ and $\tilde{Y}_C$ via

$$\tilde{Y}_m = \frac{jp + qY_m}{1 + jrY_m}, \quad m \in \{A, B, C\} \tag{8}$$

with real valued parameters *p*, *q* and *r*. However, since the same transformation applies for each of the three mode admittances, simultaneous matching of all modes cannot be achieved. If for example the admittance for mode *A* is power-matched to the input admittance of the receiver channels (i.e. $\tilde{Y}_A^* = Y_{\text{in}}$), the effective gain of the receiver channels with respect to the quasi-omni-directional pattern of mode *A* is maximized, but the effective gain for the two higher-order patterns is significantly reduced.

For the purpose of this discussion, the frequency-converted and digitised output voltages of the receiver channels are assumed to be related to the input port voltages via $V_{\text{out},n} = \alpha V_{\text{in},n}$. From a linear combination of these output voltages, an unlimited number of simultaneous beams can be formed by means of a weighted sum of these output voltages with the port-weights $\mathbf{W}^t = (W_1, W_2, W_3)$ [6]. The beamformer output voltage thus becomes (with "+" denoting transjungation)

$$V_{\text{beam}} = \alpha \mathbf{W}^+ \mathbf{V}_{\text{in}}. \tag{9}$$

With mode-weights $\mathbf{w} = \mathbf{U}^t \mathbf{W}$ where $\mathbf{U}$ is defined in eq. (2), this may be transformed into a linear combination of the input mode voltages $v_{\text{in},m}$:

$$V_{\text{beam}} = \alpha \mathbf{w}^+ \mathbf{v}_{\text{in}}. \tag{10}$$

Introducing eq. (6) and calculating $\mathbf{v}_{\text{in}}$ from the circuit shown in Fig. 5, one finds the beamformer voltage excited by an incident spectrum of homogeneous plane waves $\mathbf{E}_{\text{inc}}(\theta,\phi)$ as

$$V_{\text{beam}} = \alpha \frac{\lambda}{\sqrt{4\pi Z_0 G_{\text{in}}}} \oint \left(\sum_{m=A,B,C} w_m^* \Lambda_m \mathbf{C}_m(\theta,\phi) \right) \cdot \mathbf{E}_{\text{inc}}(\theta,\phi)\, d\Omega \,. \tag{11}$$

The effective weights for a linear combination of the eigenpatterns are thus given by

$$\tilde{w}_m = \Lambda_m^* w_m \,. \tag{12}$$

If the complex valued coefficients Λ_m are known, the weights can be adjusted in accordance with eq. (12) to account for mutual coupling. This represents a measure of compensation for mutual coupling via digital signal processing, as discussed in detail in a variety of papers [7-11].

However, this measure does not compensate for the SNR degradation due to mutual coupling. The voltages produced by the waves received by the antenna are superimposed onto noise voltages due to noise sources within the receiver channels. The noise properties of each receiver channel can be represented by a noise voltage and a noise current source (partially correlated to the noise voltage) at the input port of the receiver channel, as shown in Fig. 5. The effective receiver noise temperature T_{eff} is a function of the source admittance. The minimum receiver noise temperature $T_{\text{eff,min}}$ is achieved when the source admittance equals an optimum value $Y_{\text{opt}} = G_{\text{opt}} + jB_{\text{opt}}$. In the structure under consideration, three parallel receiver chains are connected to the mutually coupled antenna ports. Due to the mutual orthogonality of the three different modes, the noise model for each mode can be shown to be identical to the noise model for a single receiver channel. The effective noise temperature for mode *m* therefore becomes [12]

$$T_{\text{eff},m} = T_{\text{eff,min}} + T_0 R_{\text{eq}} \frac{\left| Y_m - Y_{\text{opt}} \right|^2}{G_m} \tag{13}$$

with $T_{\text{eff,min}}$, Y_{opt} and R_{eq} representing the minimum noise temperature, optimum source admittance and equivalent noise resistance of the three receiver channels, and T_0 denoting room temperature. From eq. (13), it is clear that a deviation of the mode admittance Y_m from the optimum source

admittance increases the effective noise temperature. With these results, the gain-to-noise-temperature ratio can be formulated explicitly. With a certain set of weights $\tilde{w}_m$, the ratio between the direction dependent antenna gain function $g(\theta,\phi)$ and receiver noise temperature becomes

$$\frac{g(\theta,\phi)}{T_{\text{eff}}} = \frac{\sum_{m=A,B,C} \left|\tilde{w}_m \mathbf{C}_m(\theta,\phi)\right|^2}{T_{\text{eff,min}} \sum_{m=A,B,C} \left|\tilde{w}_m\right|^2 \quad + \quad T_0 R_{\text{eq}} \sum_{m=A,B,C} \left|\tilde{w}_m\right|^2 \frac{\left|Y_m - Y_{\text{opt}}\right|^2}{G_m}} \quad . \tag{14}$$

If all mode admittances Y_m are matched to the optimum source admittance Y_{opt}, the second term in the nominator vanishes, resulting in the highest SNR. This optimum case can only be achieved if all mode admittances are identical, which necessitates the use of a decoupling network. Without a decoupling network, the mode admittances cannot be simultaneously matched to the optimum source admittance, and some modes will be badly noise-matched. If these modes are needed for forming the desired radiation characteristic, the SNR will be reduced substantially. In contrast to the correction of the weights as shown above, this effect cannot be compensated for by means of digital signal processing.

4. DECOUPLING OF ANTENNA PORTS

In order to overcome the problems described above, an RF decoupling-network (RF-DN) has to be introduced between the antenna ports and the receiver channels. For the considered configuration of three monopoles, a novel and very simple solution for this decoupling network is proposed. As seen from Fig. 3, there are two values F_1 and F_2 of the normalized frequency $F = f / f_0 = 4lf / c$ where the real parts of Y_A and Y_B are equal to each other. For a given operational center frequency f_{ctr}, the normalized frequency and thus the length l of the monopole can be adjusted to yield

$$F = \frac{4 f_{\text{ctr}} l}{c} = \begin{cases} F_1 \\ \text{or } F_2 \end{cases} \tag{15}$$

and therefore $G_{12}(f_{\text{ctr}}) = \frac{1}{3}\left[G_A(f_{\text{ctr}}) - G_B(f_{\text{ctr}})\right] = 0$. With $Y_{12}(f_{\text{ctr}}) = jB_{12}(f_{\text{ctr}})$, the decoupling network reduces to reactive cross coupling between the adjacent antenna ports. Each coupling element has an admittance of jB_{12} at the center frequency (see Fig. 6), thus yielding a 3-port admittance matrix

$$\mathbf{Y}_{\mathrm{DN}} = \begin{bmatrix} j2B_{12} & -jB_{12} & -jB_{12} \\ -jB_{12} & j2B_{12} & -jB_{12} \\ -jB_{12} & -jB_{12} & j2B_{12} \end{bmatrix} \tag{16}$$

for the RF-DN. The admittance matrix of the array and the attached decoupling network, $\tilde{\mathbf{Y}}$, then becomes

$$\tilde{\mathbf{Y}} = \mathbf{Y} + \mathbf{Y}_{\mathrm{DN}} = \begin{bmatrix} 1 & 0 & 0 \\ 0 & 1 & 0 \\ 0 & 0 & 1 \end{bmatrix} Y_A(f_{\mathrm{ctr}}) . \tag{17}$$

Each antenna port thus has an input admittance of $\tilde{Y}_{11} = Y_A = Y_{11} + j2B_{12}$ at the center frequency, irrespective of the excitation of the other ports. It therefore becomes possible to simultaneously match each port (and hence each mode) to the receiver input impedance, Y_{in} or the optimum source impedance, Y_{opt}. This may be accomplished in a straightforward manner using standard impedance matching techniques. Receiver channels are often internally noise-matched and possess a real valued input admittance Y_{in} that coincides with the characteristic admittance of cables (e.g. 1/50 Ω^{-1}). In such cases $Y_{\mathrm{opt}} = Y_{\mathrm{in}}^*$, so that optimum noise matching and power matching can be achieved simultaneously.

For the example with $a = \lambda_0/10$ and $d = \lambda_0/40$, the normalized frequency $F_1 = 0.9998$, so that the length l of the monopole needs to be decreased by 0.02% relative to $\lambda_{\mathrm{ctr}}/4$ in order to yield $Y_{12} = 0 + j0.0151\ \Omega^{-1}$ at the center frequency. If, for example, the center frequency is chosen as $f_{\mathrm{ctr}} = 2.45$ GHz, decoupling can be accomplished by connecting a capacitor of $C = 0.981$ pF between adjacent antenna ports. With this simple decoupling network, ports 1 to 3 become decoupled at f_{ctr}. This results in a decoupled port impedance of $1/\tilde{Y}_{11} = 140.3 - j2.27\,\Omega$, which may easily be transformed into the desired load impedance, e.g. $Z_{\mathrm{in}} = 50\,\Omega$. The frequency bandwidth of decoupling and matching for this case is indicated in Fig. 7, which shows the frequency response of $\left|\tilde{S}_{11}\right|^2$

(fraction of power reflected) and $2\left|\tilde{S}_{21}\right|^2$ (fraction of power coupled to the loads at the other two ports). Note that the loss due to reflection and cross coupling is theoretically zero at the center frequency. If the frequency bandwidth is defined via the requirement that 89 % of the power incident to the array is to be radiated (equivalent with the VSWR<2 bandwidth for single antennas), a fractional bandwidth of 2.6% is observed. If a wave is fed into port 1 of the new structure in Fig. 6(b) while the other two ports are terminated in matched loads, a linear combination of modes *A* and *B* is excited, resulting in a radiation pattern

$$\mathbf{C}_1(\theta,\phi) = \left(\mathbf{C}_A(\theta,\phi) + \sqrt{2}\mathbf{C}_B(\theta,\phi)\right)/\sqrt{3}\,, \tag{17}$$

with a maximum directivity of $D_1 = \left|\mathbf{C}_1\right|^2_{\max} = 10.41 \equiv 10.2$ dBi . Fig. 8 depicts the normalised azimuth pattern for $\theta = \pi/2$. If port 2 or 3 is excited, the radiation pattern is rotated about the *z*-axis by ± 120 degrees. These radiation patterns are characterized by the fact that even in direction where the maximum directivity occurs, a partially destructive interference between the field contributions of the monopole currents occurs, which is a feature of a superdirective array [1]. The monopole elements together with the RF-DN form a resonator that provides the resonant current enhancement needed for superdirective radiation properties.

5. CONCLUSION

The potential problems associated with strong mutual coupling between closely spaced array elements have been highlighted. It was shown that without a decoupling network it would be impossible to match all of the characteristic modes simultaneously. Although the effects of impedance mismatch may be compensated for in digital beamforming, the inability to compensate for the SNR degradation remains a problem that can only be solved by decoupling the array ports. For the array of three closely spaced monopoles, a novel yet simple decoupling network has been proposed.

The decoupled array represents a superdirective antenna. The drawback of superdirectivity is the frequency bandwidth limitation, which is related to the radiation quality factor Q_{rad} of the higher-

order modes. Since Q_{rad} increases with decreasing element spacing, the allowed minimum element spacing is governed by the required fractional frequency bandwidth. Furthermore, dissipative losses in the antenna and matching network structure (up to now neglected) need to be taken into account. The unloaded quality factor Q_0 of matching and antenna structure must sufficiently exceed the radiation quality factor of the high-order radiation pattern to ensure that the increased gain due to superdirectivity is not negated by a reduction in efficiency [1-3].

REFERENCES:

1. R.C. Hansen, Phased array antennas, Wiley, New York, 1998.
2. R.C. Hansen, Fundamental limitations in antennas, Proc. IEEE, Vol. 69, (1981), 170-182.
3. H.J. Chaloupka, HTS antennas, in H. Weinstock and N. Nisenoff (eds.), Microwave superconductivity, Kluwer, Dordrecht, 2001.
4. SuperNEC Lite, Version 2.0, Poynting Software Pty. Ltd.
5. IE3D, Zeland Software Inc.
6. J. Litva and T.K.Y. Lo, Digital beamforming in wireless communications, Artech House, Boston, 1996.
7. H. Steyskal and J.S. Herd, Mutual coupling compensation in small array antennas, IEEE Trans Antennas Propagat., Vol. 38, (1990), 1971-1975.
8. R.S. Adve and T.K. Sarkar, Compensation for the effects of mutual coupling on the direct data domain adaptive algorithms, IEEE. Trans. Antennas Propagation, Vol. 48, (2000), 86-94.
9. P. Darwood, P. N. Fletcher, and G.S. Hilton, Mutual coupling compensation in small planar array antennas, IEE Proc Microwaves, Antennas Propagation, Vol. 145, (1998), 1-6.
10. I.J. Gupta and A.A. Ksienski, Effect of mutual coupling on the performance of adaptive arrays, IEEE Trans Antennas Propagat., 31 (1983) , 785-791.
11. B. Friedlander and A. J. Weiss, Direction finding in the presence of mutual coupling, IEEE Trans Antennas Propagat., Vol. 39, (1991), 273-284.
12. H.A. Haus, Representation of noise in linear two-ports, Proc. IRE, (1960), 69-74.

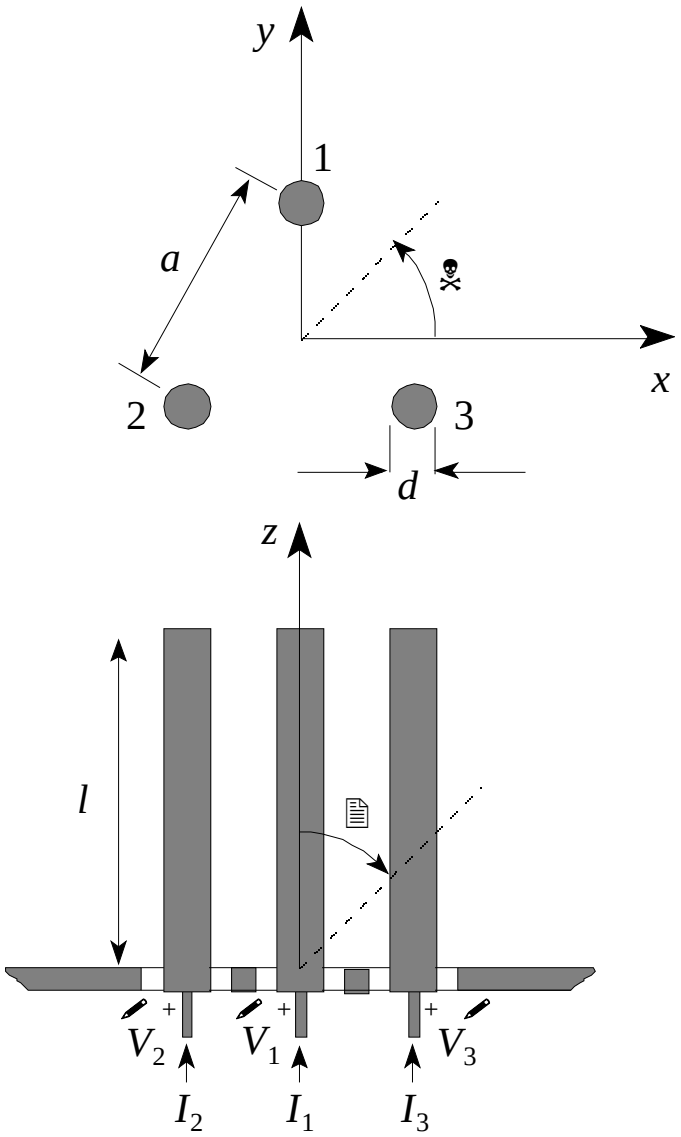

Fig.1: Considered 3-element array with monopole elements (height *l*, diameter *d*) and element spacing *a*.

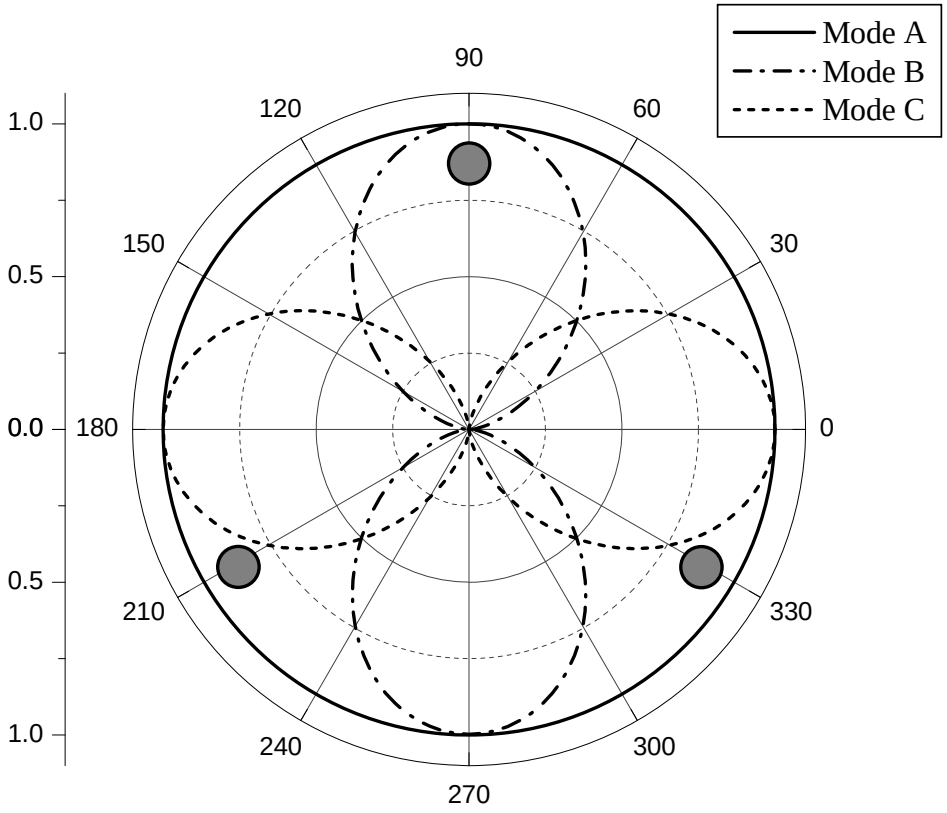

Fig. 2: Normalized radiation patterns of the three eigenmodes, $\left|\mathbf{C}_m(\pi/2,\phi)\right|/\sqrt{D_m}$, $m = A, B, C$ with maximum directivities $D_A = 3.24$, $D_B = 7.94$ and $D_C = 7.76$.

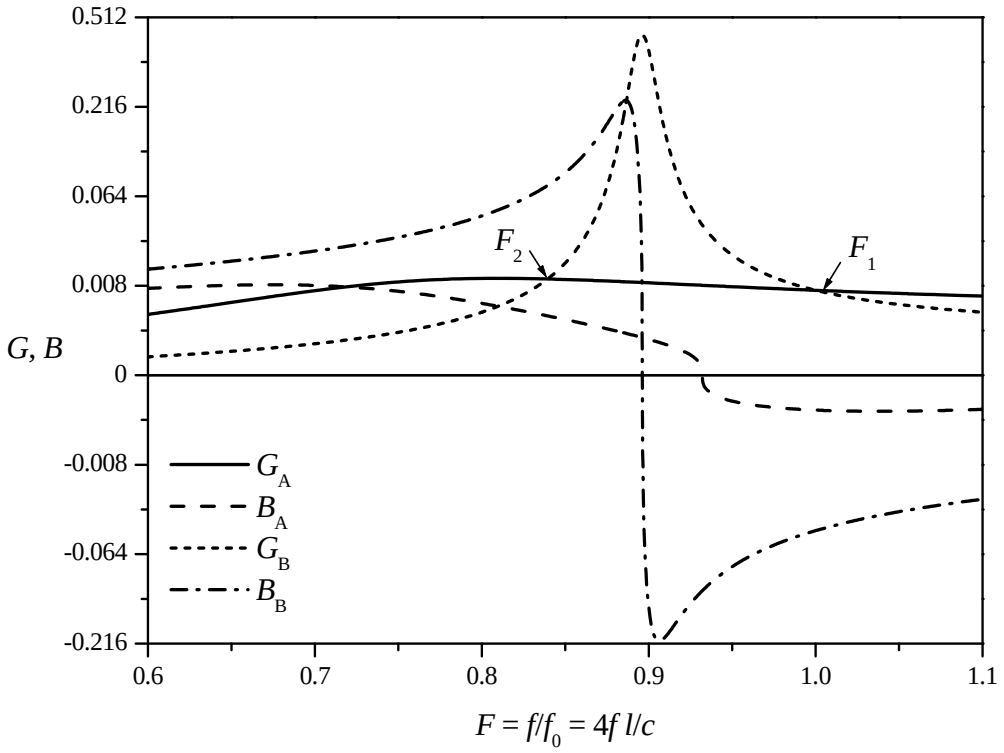

Fig. 3: Computer simulation results for the frequency response of real and imaginary part of the input admittance Y_A for the low-order and $Y_B = Y_C$ of the higher-order modes. F_1 and F_2 indicate values of the normalized frequency where the conductance $G_A = G_B$.

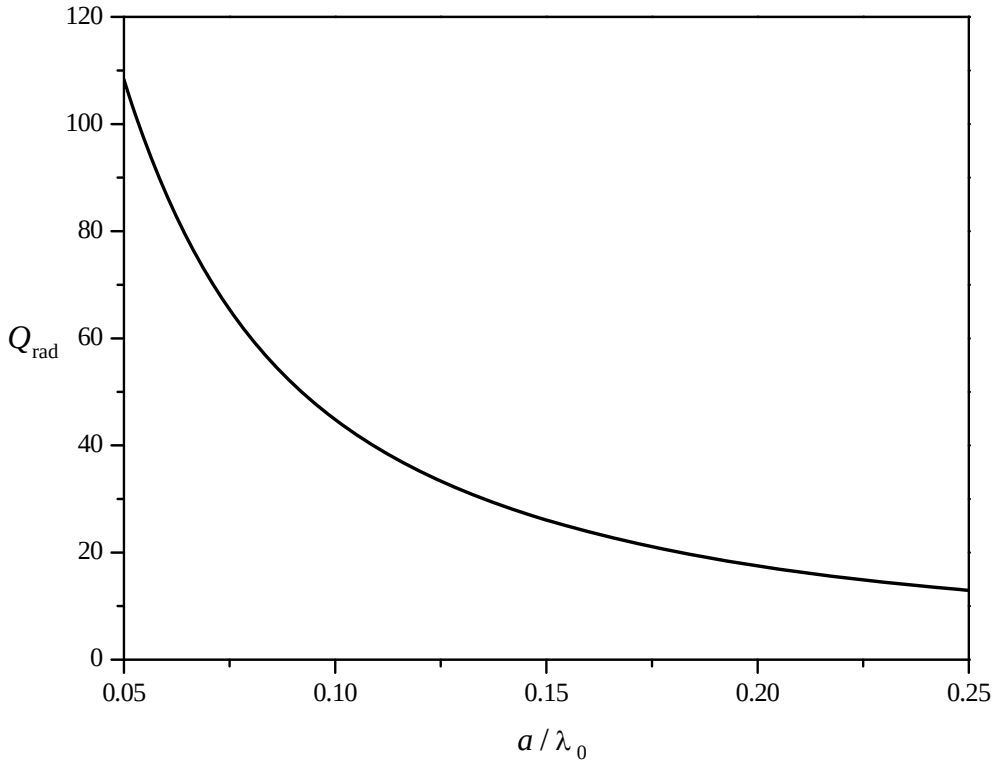

Fig.4: Dependence of the radiation quality factor of the high-order modes on the element spacing.

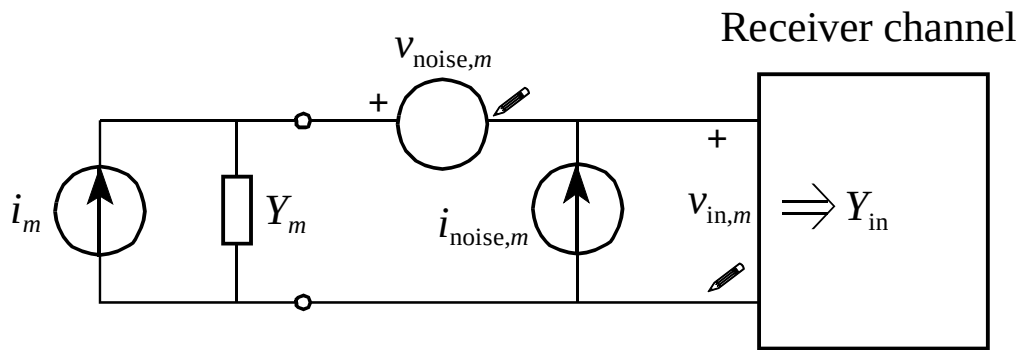

Fig. 5: Equivalent circuit for the three modes for signal-to-noise considerations:
Left: Current source representing mode *m* of the antenna array with $m \in \{A, B, C\}$.
Right: Receiver channel with equivalent noise voltage $v_{\text{noise},m}$ and noise current $i_{\text{noise},m}$.

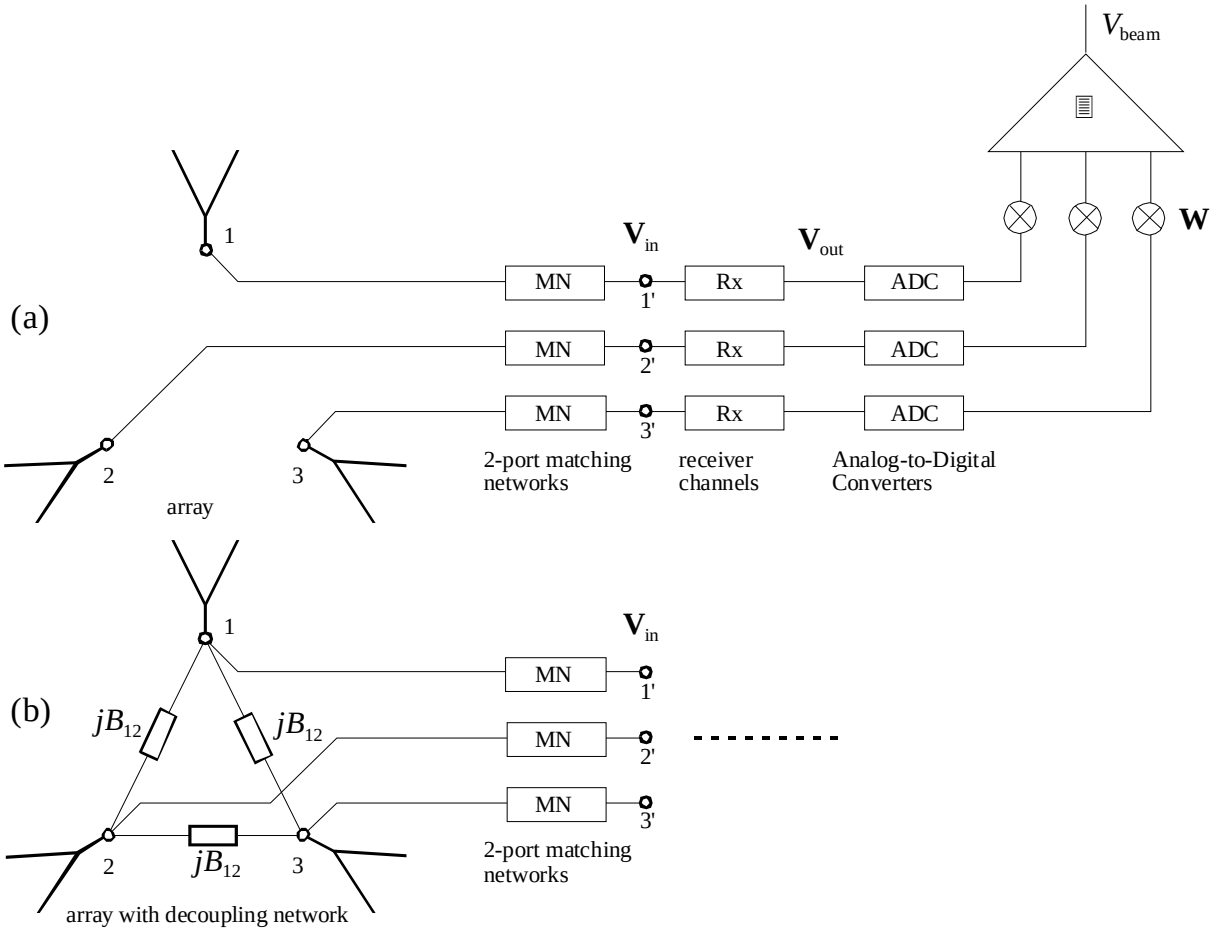

Fig. 6: Array and beamforming system (a) without and (b) with a decoupling network.

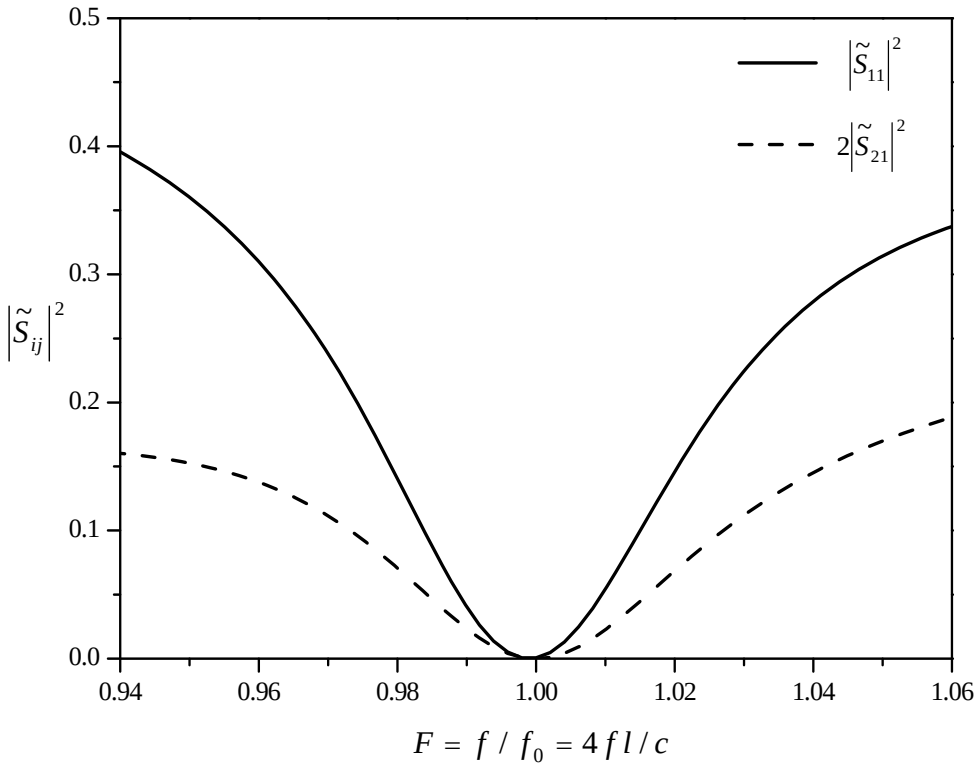

Fig. 7: Computer simulation results for the effectiveness of decoupling and matching. Shown is the fraction of power reflected and power coupled to other ports as a function of frequency when feeding one port of an array with $a/\lambda_0 = 0.1$, $d/\lambda_0 = 0.025$ and monopole length adjusted to $l/\lambda_0 = 0.24995$. Decoupling according to Fig. 6(b).

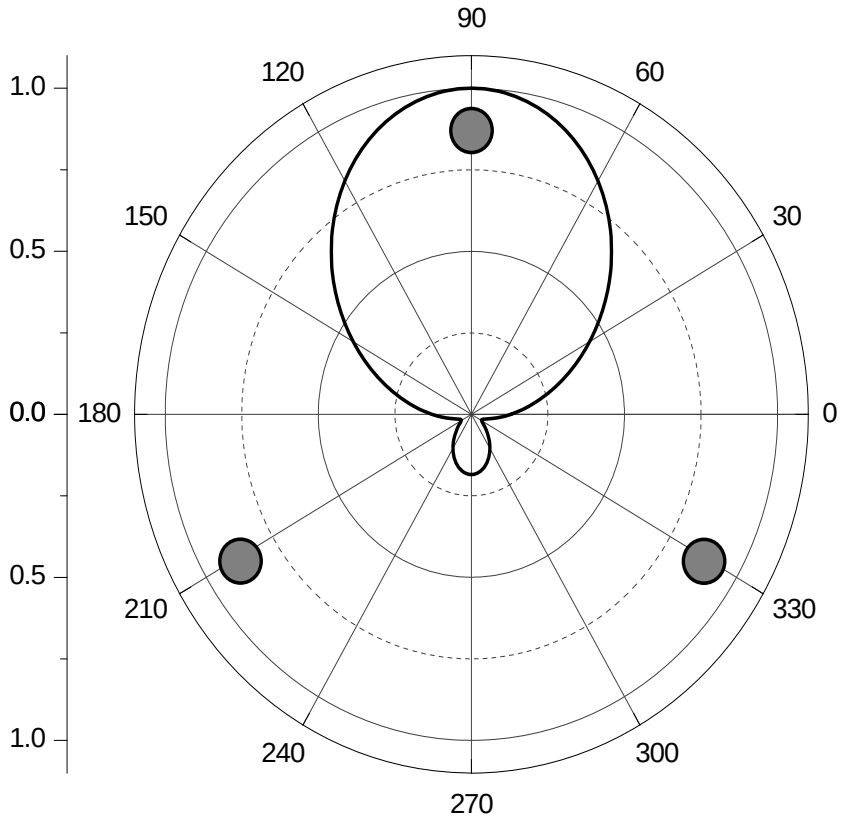

Fig. 8: Normalized radiation pattern $\left|\mathbf{C}_1(\pi/2,\phi)\right|/\sqrt{D_1}$ at center frequency f_{ctr} obtained by feeding port 1 of the 3-element array with attached decoupling network as shown in Fig. 6(b). Maximum directivity is $D_1 = 10.41$.